NeuroImage 63 (2012) 301–309

Contents lists available at SciVerse ScienceDirect

NeuroImage

journal homepage: www.elsevier.com/locate/ynimg

Technical Note

Simultaneous intracranial EEG–fMRI in humans: Protocol considerations and data quality

D.W. Carmichael [a,b,*], S. Vulliemoz [b,c], R. Rodionov [b], J.S. Thornton [d], A.W. McEvoy [e], L. Lemieux [b]

[a] Imaging and Biophysics Unit, UCL Institute of Child Health, 30 Guilford Street, London, WC1N 1EH, UK
[b] Department of Clinical and Experimental Epilepsy, UCL Institute of Neurology, Queen Square, London, WC1E 6BT, UK
[c] Epilepsy Unit, Neurology Department, University Hospital and University of Geneva, 1211 Geneva 14, Switzerland
[d] Lysholm Department of Neuroradiology, National Hospital for Neurology and Neurosurgery, Queen Square, London, WC1N 3BG, UK
[e] Victor Horsley Department of Neurosurgery, National Hospital for Neurology and Neurosurgery, Queen Square, London, WC1N 3BG, UK

ARTICLE INFO

Article history:
Accepted 21 May 2012
Available online 29 May 2012

Keywords:
EEG–fMRI
Intracranial EEG
Functional MRI
fMRI
Data quality
icEEG–fMRI
Electrophysiology
BOLD
Simultaneous EEG and fMRI

ABSTRACT

We have recently performed simultaneous intracranial EEG and fMRI recordings (icEEG–fMRI) in patients with epilepsy. In this technical note, we examine limited thermometric data for potential electrode heating during our protocol and found that heating was ≤0.1 °C in-vitro at least 10 fold less than in-vivo limits. We quantify EEG quality, which can be degraded by MRI scanner-induced artefacts, and fMRI image (gradient echo echo-planar imaging: GE-EPI) signal quality around the electrodes, which can be degraded by electrode interactions with B1 (radiofrequency) and B0 (static) magnetic fields. We recorded EEG outside and within the MRI scanner with and without scanning. EEG quality was largely preserved during scanning and in particular heartbeat-related artefacts were small compared to epileptic events. To assess the GE-EPI signal reduction around the electrodes, we compared image signal intensity along paths into the brain normal to its surface originating from the individual platinum–iridium electrode contacts. GE-EPI images were obtained at 1.5 T with an echo time (TE) of 40 ms and repetition time (TR) of 3000 ms and a slice thickness of 2.5 mm. We found that GE-EPI signal intensity reduction was confined to a 10 mm radius and that it was reduced on average by less than 50% at 5 mm from the electrode contacts. The GE-EPI image signal reduction also varied with electrode orientation relative to the MRI scanner axes; in particular, cortical grid contacts with a normal along the scanner's main magnetic field (B_0) axis have higher artefact levels relative to those with a normal perpendicular to the z-axis. This suggests that the artefacts were predominantly susceptibility-related rather than due to B1 interactions. This information can be used to guide interpretation of results of icEEG–fMRI experiments proximal to the electrodes, and to optimise artefact reduction strategies.

© 2012 Elsevier Inc. All rights reserved.

Introduction

We have recently reported the first simultaneous intracranial EEG and fMRI (icEEG–fMRI) experiments in humans which were obtained in patients with epilepsy with the aim of mapping and characterising the brain areas associated with epileptic discharges (Vulliemoz et al., 2011). The main technical challenges of recording intracranial EEG (icEEG) and fMRI simultaneously (icEEG–fMRI) are patient safety (Carmichael et al., 2010), MRI scanner-induced EEG artefacts (Allen et al., 1998, 2000) and fMRI image quality degradation (Vulliemoz et al., 2011).

Initial experimental results were encouraging in that the quality of intracranial EEG recorded during fMRI was good based on visual assessment and many more events were detected as compared to scalp EEG–fMRI recordings in the same patients (Vulliemoz et al., 2011), as expected from studies of intracranial and scalp EEG (Tao et al., 2005). However, in order to fully exploit the greater sensitivity of icEEG every effort must be made to capture the electrophysiological activity occurring across a wide frequency range and small spatial scale with minimum contamination from interactions between the EEG and scanning processes. Responses linked to epileptic events were detected within a centimetre of electrode contacts, but there was loss of GE-EPI signal proximal to each electrode contact (Vulliemoz et al., 2011). Visual assessment of the fMRI image data obtained in those studies showed that the extent of the GE-EPI signal loss was dependent on electrode type and location. These observations motivate a more quantitative characterisation of the imaging artefacts.

In this work, we report in-vitro temperature measurements with our study protocol performed prior to patient studies, quantify both the effect of scanning on EEG using spectral analysis and the effect of electrodes on GE-EPI signal intensity in patient data. For the latter, we considered the following factors: electrode type (grid, depth), distance from the electrode, anatomical localisation, and orientation of the

* Corresponding author at: Imaging and Biophysics Unit, UCL Institute of Child Health, 30 Guilford Street, London, WC1N 1EH, UK. Fax: +44 2079052358.
E-mail address: d.carmichael@ucl.ac.uk (D.W. Carmichael).

1053-8119/$ – see front matter © 2012 Elsevier Inc. All rights reserved.
doi:10.1016/j.neuroimage.2012.05.056

electrode relative to the MRI scanner's main magnetic field (B_0, and by convention the z-axis).

Methods

In-vitro RF heating safety testing

This set of experiments was designed to complement previously published studies by considering new electrode connection configurations and to determine likely heating effects in the actual configuration used in subsequent patient studies. We previously studied heating in experiments where the electrodes were either all not connected (Carmichael et al., 2008a) or all connected to the EEG recording amplifier (Carmichael et al., 2010). Our MR compatible EEG system can record up to 64 channels but patients at our centre are sometimes implanted with more contacts. We therefore conducted new experiments with some electrodes not connected but electrically isolated and configured as in Fig. 1, corresponding to the situation whereby scanning is performed while recording from a subset of the implanted electrode contacts.

We used the same experimental methods, EEG amplifier and cable configurations within the MRI scanner expected to minimise heating from our previous studies (Carmichael et al., 2008a, 2010). In summary, this entails the positioning of a large number of electrode types in different locations within a head and torso sized test object containing gel with electric conductivity and thermal properties that are similar to body tissue (Carmichael et al., 2007, 2008a). Two depth electrodes were used: 1 SD-8PX (8 electrode contacts, numbered #1–8 with 10 mm spacing, total length 380 mm), 1 SD-6PX (6 electrode contacts, numbered #1–6 with 10 mm spacing, total length 370 mm). One grid electrode array (also Ad-Tech, Racine, WI) was investigated: 1T-WS-48PX grid (6×8 contacts with 10 mm spacing, numbered #1–48 and 6 tails, one for each strip of 8 contacts, total length 455 mm). Each grid contact consists of a 4 mm diameter platinum–iridium disk (2.3 mm exposed) imbedded within a silicon sheet with stainless steel (316) wires and nickel–chromium tail contacts contained within polyurethane tubing.

For experiments below, the 2 depth electrodes and 1 subdural grid described above were positioned within the "head" region of the phantom. The depth electrodes were inserted along the left–right axis and perpendicularly to the sagittal plane, left hand side (LHS) (1×8 contacts) and right hand side (RHS) (1×6 contacts). This simulated implants targeting the left and right hippocampus. The electrodes' leads were run along the phantom wall (within the gel) for 40 mm before exiting the phantom to simulate surgical implantation with electrode-leads tunnelled under the skin away from the cranial window to avoid infection. The lead lengths inside/outside the phantom for the grid electrode were 155/300 mm, for the RHS depth electrode 120/250 mm, and for the LHS depth electrode 115/265 mm. The subdural grid electrode array was positioned so as to simulate implants recording from the cortical surface. We manufactured a foam insert with indentations to ensure highly reproducible and secure placement of all the external components of the icEEG recording system in the MRI scanner bore (Fig. 1). We executed identical pulse sequences to those used in subsequent patient studies (see below for the details of each sequence). We additionally performed a high SAR fast spin echo scan (SAR 3.0 W/kg, 6 min) deliberately designed to provoke significant heating. We recorded the temperature during the entire scanning protocol at four locations; the two distal contacts of the depth electrodes on the left hand side and right hand side of the phantom and the grid corners — contacts #1 and #41 (see Carmichael et al., 2010, Fig. 3). We used a fibre optic system (Model 3100, Luxtron Corporation, Santa Clara, CA, USA; accuracy ± 0.1 °C) during the MRI acquisition protocol to measure temperature changes. We tested the set-up with all contacts connected to the amplifier and then removed the cable for grid contacts 1–8, then additionally the cable for grid contacts 41–48 and the left hand side depth electrode cable, then contacts grid 41–48 and both left and right hand side depth electrodes.

In-vivo studies of EEG and MR image data quality

Two patients with refractory focal epilepsy were studied (see Vulliemoz et al., 2011 for details) following a comprehensive safety assessment, approval from our institutional ethical review committee (Joint UCL/UCLH), and written informed consent from the participants. Intracranial electrodes (all from Ad-Tech, Racine, WI) were implanted solely for the purpose of clinical assessment for epilepsy surgery as follows: patient #1 had one subdural grid (6×8 contacts, T-WS-48BPX) placed over the lateral left frontal lobe (red disks in Fig. 2a) and subdural strips placed below the grid (one strip with 2×8 contacts, T-WS-16PX, green disks in Fig. 2a) and anterior to the grid (two strips with 1×6 contacts, T-WS-6-PX, blue disks in Fig. 2a — only one strip electrode is shown); patient #2 had two depth electrodes (1×6 contacts, SD-6PX, orange and yellow disks show entry points in Fig. 2b) placed in a lateral–medial orientation targeting the left amygdale and hippocampus; one subdural grid (4×8 contacts, T-WS-32PX, green disks in Fig. 2b) over the left lateral temporal cortex; three subdural strips (1×8 contacts, T-WS-8-PX) under the temporal lobe (anterior 'SA', middle 'SB', posterior 'S'; pink, red and dark red disks in Fig. 2b); one subdural strip (2×8

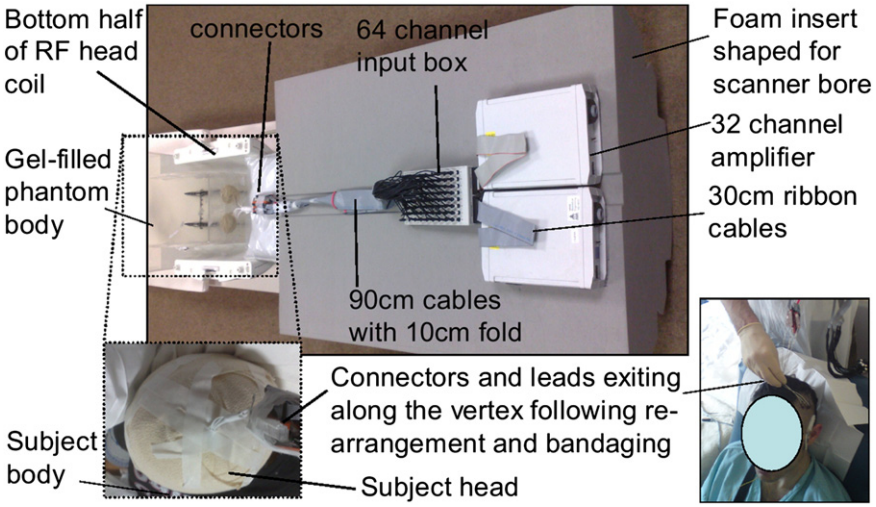

Fig. 1. EEG equipment configuration used for safety testing and subsequent patient studies. For patient studies all the electrode cables were arranged in the same configuration as for in-vitro testing from the vertex along the head foot axis of the patient. Gauze pads were placed between the external section of the electrode cables and the skin.

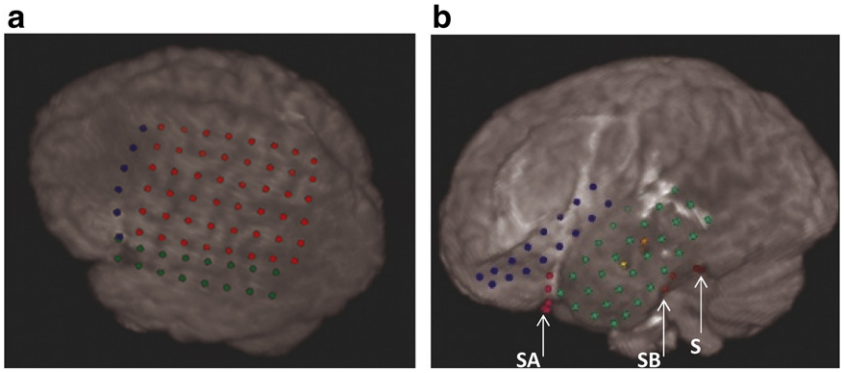

Fig. 2. Electrode contacts implantation. Electrode contacts are visualised by overlaying them on the brain surface derived from the T1-weighted structural volume for a) patient #1 and b) patient #2.

contacts, T-WS-16-PX, blue disks in Fig. 2b) over the inferior frontal cortex.

Data acquisition

MRI studies were performed at 1.5 T on a TIM Avanto MRI scanner (Siemens, Erlangen, Germany) running software version VB15, with a quadrature head transmit–receive RF coil using low specific absorption rate (SAR) sequences (≤0.1 W/kg head average). Both low SAR scans and a head transmit coil are important factors in reducing the risk of RF induced heating (Carmichael et al., 2010). Patients were asked to report any unusual or uncomfortable sensation via the in-scanner patient alarm.

The following scans were performed in both patients and in-vitro:

1) Localiser: Siemens 'fl2d1' 2D multi slice gradient echo scan with the following parameters TR/TE/flip angle 8.6 ms/4 ms/20° 15×7 mm slices with 1.4 mm gap and 256×205 in-plane acquisition matrix; field of view 250×250 mm; scan duration: 26 s.
2) T1 weighted structural scan: Siemens 'fl3d1' FLASH T1-weighted 3D structural volume, TR/TE/flip angle = 15 ms/4.49 ms/25°, resolution 1.0×1.2×1.2 mm, FoV 260×211×170 mm, 256×176×142 image acquisition matrix with the readout direction lying in the sagittal plane; duration: 6 min 15 s.
3) Gradient echo EPI (GE-EPI) 'resting' fMRI scan: Siemens 'epfid2d1_64' TR/TE/flip angle = 3000 ms/40 ms/90°, 64×64 acquisition matrix, 38×2.5 mm slices with 0.5 mm gap, standard fat selective saturation pulses were used prior to each slice. 200 volume repetitions; duration: 10 min. For in-vivo scans the subject was asked to lie still with eyes closed. Two sessions were recorded for each patient.

The following scan was performed in patient #1:

4) Gradient echo EPI (GE-EPI) 'task' fMRI scan. All scan parameters were the same as scan '3' except that only 105 volume repetitions were obtained instead of 200; duration 5 min 15 s. The patient was visually cued to touch their thumb to each finger in succession on their left hand followed by the same motor task on their right hand in blocks of 30 s duration for each hand. This scan was obtained in patient #1 only, based on the implantation given that electrode coverage included the primary sensorimotor cortex allowing the opportunity to test for fMRI responses close to the electrode contacts.

This series of scans constitutes our icEEG–fMRI scanning protocol for use in patients. No other MR sequence was allowed, except additional repetitions of the same fMRI pulse sequence (Carmichael, 2010; Bennett et al., 1996) according to the experimental circumstances.

EEG was recorded using a 2×32 channel MR compatible system located at the head end of the scanner and ECG was recorded using a 16 bipolar channel "ExG" MR-compatible system located at the patient's feet. The EEG instrumentation was placed on the anti-static foam (as per Fig. 1) insert located at 'head' end of the scanner bore (Fig. 1). Carbon fibre leads placed remotely from the icEEG recording lead were used for the ECG recording to prevent potential interactions; both types of electrophysiological signal were recorded using Brain Recorder (Brain Products, Gilching, Germany). Recordings sampled at 5000 Hz with subsequent filtering and down sampling to 250 Hz.

Computed tomography (CT) scans were acquired shortly following the implantation of the icEEG electrodes, and prior to the icEEG–fMRI session, as part of the patients' clinical management.

Data processing and analysis

In vitro assessment of scanner induced RF heating

Temperatures at each measurement location were recorded continuously at a rate of approximately 0.5 Hz. The maximum temperature increases relative to mean baseline within this period were determined from 1 min prior to MR scanning (baseline period) to 4 min after the end of scanning. We verified that the temperature sensors were working correctly using a high SAR (3.0 W/kg head average; not part of our patient scan protocol) fast spin echo scan chosen to deliberately provoke a measurable temperature change.

Assessment of icEEG quality

Scanning-related artefacts on EEG were removed using the Brain Analyser V1.3 (Brain Products, Gilching, Germany) implementation of the template subtraction and filtering algorithm (Allen et al., 1998, 2000). We retrospectively compared icEEG data under different recording conditions; a) outside the MRI scanner, b) inside the MRI scanner (no scanning) and c) inside the MRI scanner (scanning with GE-EPI). We compared power at different spectral frequencies aiming to determine if they were contaminated by residual MRI-related artefacts. For this analysis we chose to compare ten epochs of 10 s duration in each condition to enable sufficient averaging across brain states to minimise any neurophysiologic differences between the recording periods. The icEEG data recorded were reviewed retrospectively showing that only patient #2 had sufficient data (100 s) recorded in all the conditions. We selected the following 3 electrode contacts for comparison; the 1st contact on the hippocampal depth electrode being the most active (frequent high amplitude epileptic discharges) depth electrode contact; the first contact on both the most anterior strip electrode being the most active subdural contact; the most basal of the strip electrodes being an inactive subdural contact. This choice was made a priori to be a representative summary in view of the large number of electrodes. Ten epochs of 10 s duration were entered into an ANOVA to test for differences in band power across the three electrodes and six frequency-bands used above. Significance was taken to be $p<0.05$ Bonferroni corrected to account for

(n = 18) multiple comparisons between electrode contacts and bands.

Assessment of fMRI responses

Only fMRI data from the motor task session in patient #1 were considered in this first analysis; a motor task was only performed in patient #1 due to the frontal electrode coverage. The presence of significant task-related fMRI changes was assessed voxel by voxel over the whole field of view using spm5 software (www.fil.ion.ucl.ac.uk/spm) in Matlab (www.mathworks.com). All GE-EPI images were realigned to the first image and spatially smoothed (FWHM 8 mm). For the five-minute finger tap task a standard block design was used in a general linear model with motion effects modelled as the six realignment parameters and a voxel-wise statistical threshold of $p<0.05$ family wise error corrected for multiple comparisons across voxels was applied to the SPM{t} maps.

Assessment of GE-EPI signal loss

In both patients, the CT, structural volume and mean GE-EPI image (following a 2-pass realignment procedure as implemented in spm5) were co-registered and the electrode locations thus visually identified within the image-space of the mean GE-EPI. This allowed us to represent the cortical grids as 3rd order polynomial surfaces, fitted to the electrode contact locations using a least squares procedure. For the purpose of quantifying the GE-EPI signal intensity local to the electrode contacts, the normal to the grid surface at each contact location was defined. A virtual path was created that projected from each contact along the local surface normal 30 mm into the brain. For depth electrodes, which are approximately straight and orientated towards the centre of the brain, radial paths emanating from each contact were defined within planes centred at each contact location and perpendicular to the long axis of the electrode trajectory. The mean, standard deviation and range of the GE-EPI signal magnitude were calculated as a function of the distance from the electrode contact along these paths. The surface normal at each contact was used to define its angle relative to the main magnetic field. Signal intensity was assessed every 1 mm along these paths by spline interpolation of the mean of the realigned GE-EPI image volume.

Results

In vitro temperature measurements

Temperature variations during the entire scanning protocol used for in-vivo experiments (≤0.1 W/kg head average SAR) were below the resolution of our temperature measurement system (≤0.1 °C). Temperature changes of maximum value 1.5 °C were measured when a high SAR (3.0 W/kg head average) sequence was used. Temperature changes were not increased by partially connecting electrode contacts to the EEG amplifier leaving the remaining electrodes unconnected (but electrically isolated). Temperature data are provided in Table 1 and Supplementary Figs. S1 and S2.

icEEG data quality

Post-hoc correction of the EEG (Allen et al., 2000) was necessary to reduce the scanning-related artefacts, resulting in good EEG upon visual inspection (Figs. 3c and d). The amplitude of the pulse-related artefact was low (below 5% of typical epileptic discharges see Fig. 4a). Of the 18 contact and frequency-band combinations tested (patient #2 only) only power in the low gamma band was significantly altered ($p<0.05$ Bonferroni corrected) during scanning following correction for gradient artefacts compared to data recorded outside the MRI scanner (Fig. 4b).

Table 1
Temperature changes recorded at 4 locations during in-vitro testing with a high SAR (3.0 W/kg head average) sequence. The experiment was repeated with different combinations of electrodes connected to the amplifier.

Run	Electrode contacts with cables to amplifier removed	Measurement location			
		Left depth contact #1	Right depth contact #1	Grid contact #1	Grid contact #41
1	None	1.2	1.5	1.1	0.3
2	Grid contacts #1–8	1.1	1.4	0.8	0.8
3	Grid contacts #1–8, #41–48, left depth	0.1	0.6	0.3	0.8
4	Grid #41–48, left and right depths	0.2	0.1	0.5	0.4

MRI data quality

T1-weighted structural images show the location of many of the electrode contacts via small regions of signal loss. The brain's sulci and gyri are clearly visible when surface-rendered beneath the grid of intracranial electrode contacts (derived from a coregistered CT image) as shown in Fig. 2. Representative MRI data from patient #1 is shown in Fig. 3a and patient #2 in Fig. 3b. For the finger-tapping task (patient #1 only due to electrode coverage) a strong positive fMRI response was found close to the electrode grid contacts; the estimated distance from the activated region to the nearest contact was 2 mm, i.e. in the adjacent voxel.

For patient #2, the region of significant GE-EPI signal loss was generally more extensive especially around the depth electrode contacts and the strip electrodes underneath the temporal pole.

In patient #1, the frontal electrode coverage including primary sensory and motor regions can be visualised when overlaid on the post-implantation volume (Fig. 5a). Under the cortical electrode grid (red contacts in Fig. 2a) there was no GE-EPI signal loss at 10 mm from any contacts and an average of 30% signal loss at 5 mm, but with considerable variability between contacts (Fig. 5b). Assessment of the GE-EPI signal loss at 5 mm as a function of the electrode orientation relative to the MRI scanner axes (Fig. 5c) revealed greater reductions for contacts with a vector normal to the grid surface parallel to B_0. This corresponds to electrode contacts on the brain surface lying in the x–y plane of the MRI scanner as by convention B_0 lies along the scanners z-axis, with the x-axis being the left–right axis (in a standard axial head image). There was less GE-EPI signal loss around contacts that were at 90° to the B_0 field (i.e. for electrode contacts lying in the z–y plane). We also observed an effect as the angle of the surface normal relative to the scanner y-axis (anterior–posterior in a standard axial head image) was increased above 90° with greater signal loss seen at 5 mm from the more posterior contacts. This might be related to increased distortions and dropout associated with susceptibility-related magnetic gradient fields in the phase-encoding direction (here the y-axis) that are altered as the electrode contact is rotated about the z-axis.

A similar pattern of GE-EPI signal loss was found in patient #2 (Fig. 6) for a grid placed over the temporal lobe (green contacts in Fig. 6a) with no signal loss at 10 mm from any contact and around 30% loss at 5 mm (Fig. 6b). The variability in GE-EPI signal loss between contacts was greater than in patient #1 due to the increased brain surface curvature at the temporal pole (Fig. 6c). For the depth electrodes, targeting the left amygdale and hippocampus respectively, the GE-EPI signal levels along radii emanating from the individual contacts can be visualised in Fig. 6b. These plots showed a similar pattern to the equivalent plots for electrode grid contacts; that the GE-EPI signal was reduced closer to the electrode contacts with an average full signal found within 10 mm with >50% of the full signal at 5 mm from the depth electrode contacts.

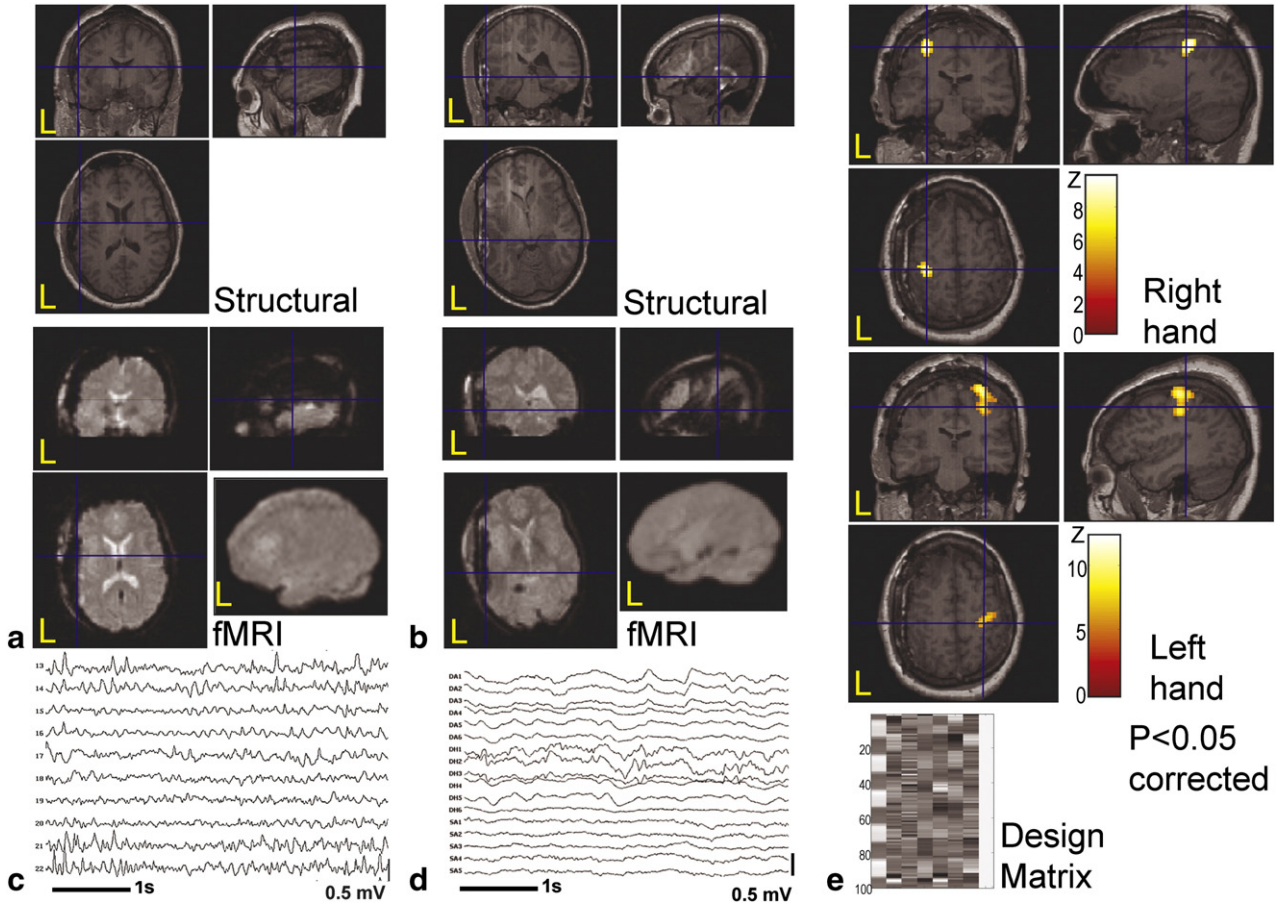

Fig. 3. Simultaneously acquired MRI and icEEG data quality; visual comparison. The same three orthogonal views are displayed of MRI structural (top left) and fMRI data (bottom middle left) in patient #1. The cross hairs indicate the displayed slices through the volume and are centred near the implanted electrode contacts. These are displayed overlaid on the reconstructed brain surface from the T1-weighted volumetric MRI. The fMRI data volume (bottom left) is also surface reconstructed to visualise image artefact levels. As in 'a' for patient #2. A segment of MRI scanner artefact corrected icEEG for patient #1. As in 'c' for patient #2. The results of the left vs. right hand finger tap task in patient #1 with the fMRI response visible immediately beneath the electrode contacts on the cortical surface.

Discussion

We have quantified EEG and image quality in simultaneously acquired intracranial EEG and fMRI data in humans, to further demonstrate the technique's potential and limitations and set a baseline for possible future developments aimed at improving data quality. We have also described additional temperature measurements we performed to extend our previous studies, and confirm that our patient protocol avoided excessive heating for realistic electrode-lead configurations.

Patient safety

An experimental protocol for use in patients was designed and tested based on our previous experiments to minimise the risk of RF heating (Carmichael et al., 2008a, 2010). In summary, we used a 1.5 T MRI scanner with a head transmit–receive coil and low specific absorption rate (SAR ≤ 0.1 W/kg head average) sequences. Scanner calculated SAR values obtained in each patient for the scan protocol are shown in Table 2. Leads and wires external to the head were maintained with specific lengths and precise positioning along the RF coil's central z-axis. We aimed to test heating levels expected in-vivo following this protocol using in-vitro experiments. We therefore performed the presented test scans using our patient protocol, which was devised based on previous in-vitro work, rather than with scans and durations that would provoke the greatest or 'worst case' temperature increases. Longer scans may produce greater heating in-vitro although a scan duration of 6 min is thought to be the duration required to reach equilibrium temperatures in-vivo (Carmichael et al., 2010). Heating was limited to ≤0.1 °C, implying that a safety factor of 10 in relation to the statutory temperature increases limits (+1 °C) (International Electrotechnical Commission (IEC), 2002) and of approximately 50 for actual tissue damage (Dewhirst et al., 2003), although this depends on exposure duration. This margin of safety represents a conservative approach determined by the potential differences between patient and in-vitro studies with associated uncertainties in heating within a particular patient (Carmichael et al., 2008a, 2010).

In addition, we tested configurations where only a subset of electrodes was connected. These were consistent with our previous studies (Carmichael et al., 2008a, 2010) showing that the configuration of cabling can make a difference to the heating at a particular location. However, removing a cable connection to a particular electrode (while maintaining all other conditions such as electrode tail path) did not increase the peak temperature recorded. In-vitro studies can be limited by temperature measurement accuracy (Mattei et al., 2007) although sufficient reproducibility is possible (Carmichael et al., 2008a). We cannot exclude the possibility that temperature changes above those recorded were present in other locations that were not sampled. We presumed the measured locations to be among the most likely to exhibit heating from our previous experience (Carmichael et al., 2007; Carmichael et al., 2008a, 2008b, 2010). However given the wide range of tested configurations covered by this work and our two previous studies (Carmichael et al.,

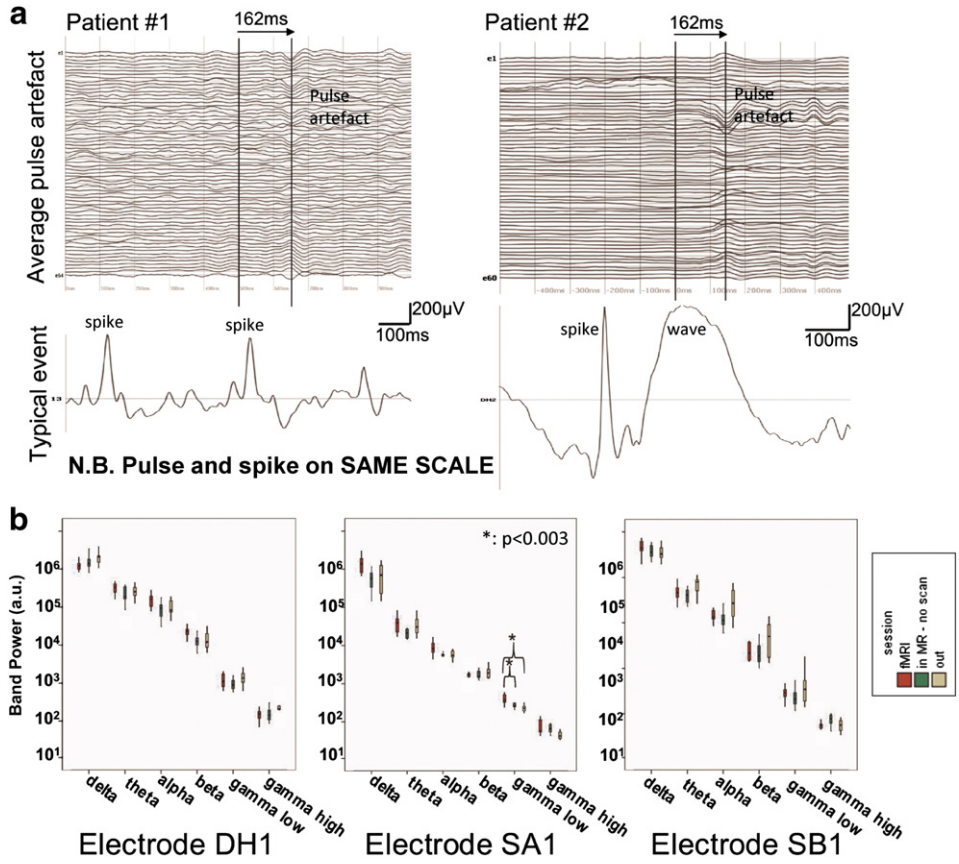

Fig. 4. Quantitative evaluation of the icEEG. The average cardiac-related artefact obtained for each patient and channel is compared to typical epileptic discharges in each patient. N.B. The average pulse artefact and epileptic discharges are shown on the same scale. Spectral changes in icEEG induced by the MRI environment. DH1: Left hippocampal depth electrode contact with maximal epileptic activity. SA1: Left basal temporal electrode contact with no epileptic activity. SB1: Left basal temporal subdural electrode contact with maximal epileptic activity. Each spectral band is compared in each condition (see key) for each contact the error bars show standard deviation. The only statistically significant change is an increase in low gamma power caused by artefacts/correction in one electrode ($p<0.05$ Bonferroni corrected for 6 bands and 3 electrodes = $p<0.003$).

2008a, 2010) it is unlikely that dramatically larger temperature changes than those measured here could result and the safety margin we have used within our patient protocol should account for these potential measurement inaccuracies.

We also closely monitored the patients before, during, and after scanning and reviewed MRI scans, intra-operative photos and histology reports where available in addition to visual inspection of the exposed brain surface where possible before and after icEEG–fMRI to verify that scanning related injury had not occurred. Some surgical trauma is inevitable during electrode implantation hence relying on experimental safety assessments and a wide safety margin should be preferable to potentially ambiguous post-hoc analysis. We emphasise that the safety

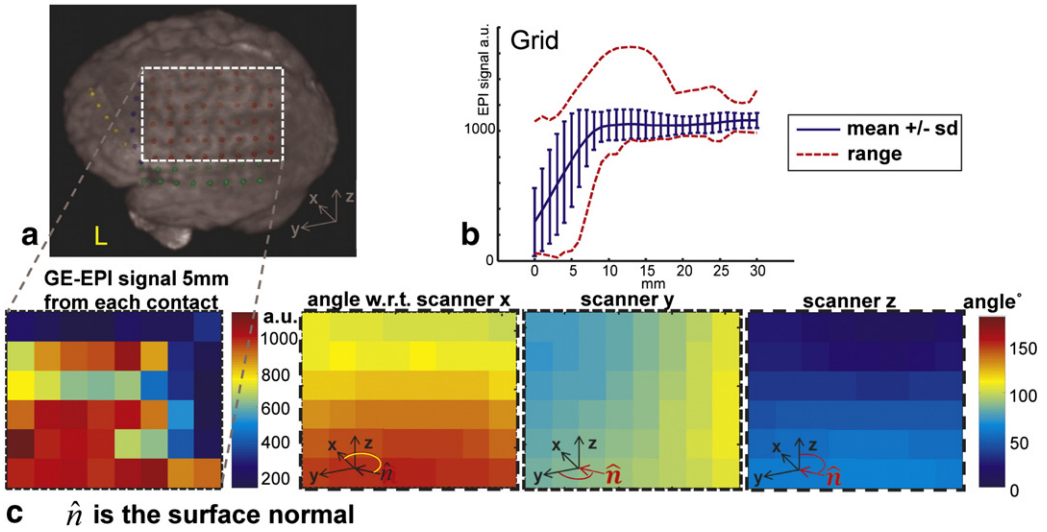

Fig. 5. Quantitative evaluation of electrode related MRI signal reduction patient #1. The cortical surface contacts used for part 'c' are shown using the dashed-line box on a rendered MRI structural scan with electrodes overlaid. The profiles of the GE-EPI signal with distance from the grid electrode contacts into the brain. The signal level at 5 mm from each contact (1 pixel) is compared to the angle of the contact with surface normal n̂ relative to each of the scanner axes.

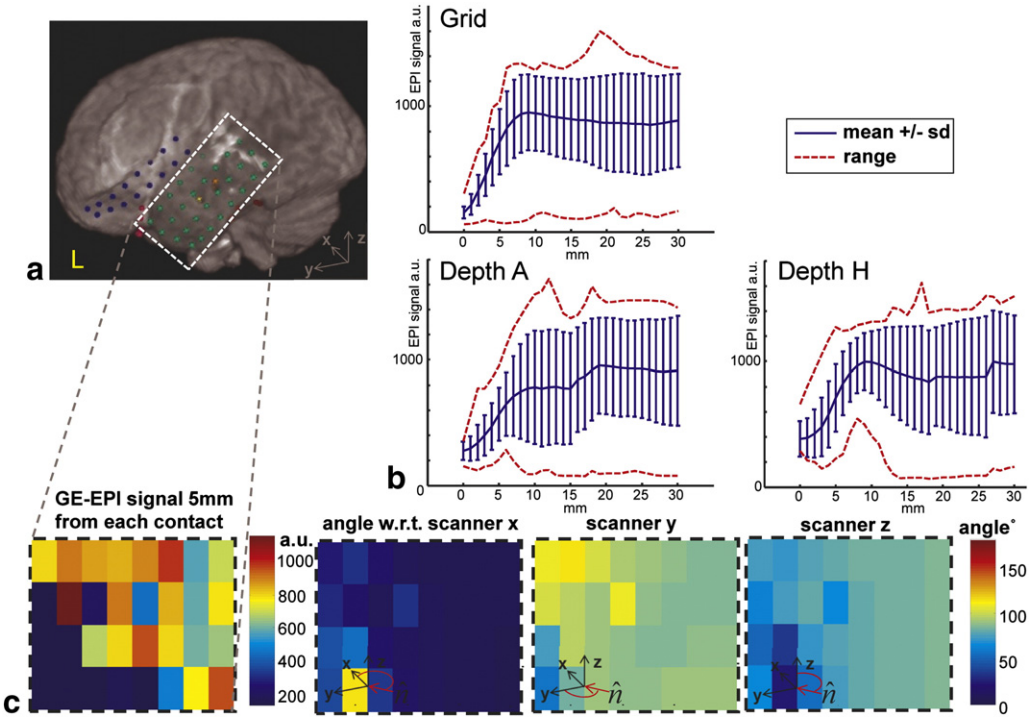

Fig. 6. Quantitative evaluation of electrode related MRI signal reduction patient #2. The cortical surface contacts used for part 'c' are shown using the dashed-line box on a rendered MRI structural scan with electrodes overlaid. The profiles of the GE-EPI signal with distance from the grid and depth electrode contacts into the brain are shown. The signal level at 5 mm from each contact (1 pixel) is compared to the angle of the surface normal $\hat{n}$ relative to each of the scanner axes.

risk associated with performing icEEG–fMRI is scanner hardware and software dependent: field strength, RF transmit coil type and design, and imaging pulse sequence design can all potentially alter the level of heating. Local testing is therefore important to establish the potential for RF-induced heating at a particular site.

EEG data quality

Following correction for MRI gradient-artefacts, icEEG data quality was generally visually and quantitatively comparable to that of icEEG recorded outside the MRI scanner. We found only one significant scanning-related difference in the low gamma frequency-band in one electrode contact from the three electrodes and six frequency-bands tested. Such differences may be attributable to imperfect gradient artefact correction or differences in brain state between the recordings; this needs to be studied in a larger dataset. Our results suggest that spectral information can be accurately quantified for most of the spectrum. The heart beat-related artefact found in scalp EEG recordings performed within the MRI scanner's strong static magnetic field (Allen et al., 1998), was also present in the icEEG signals but was typically 10–20 times smaller in magnitude relative to icEEG signals of interest from the brain (e.g. epileptic discharges), and were not large enough to cause systematic differences in band-power (Fig. 4b) so their correction might not always be required.

Table 2
SAR values recorded during in-vivo studies.

	Scan	Duration (s)	SAR (W/kg, head-average)
Patient #1	Localiser	30	0.03
	Structural	375	0.13
	Resting fMRI	600	0.13
	Finger tap task	315	0.13
Patient #2	Localiser	30	0.03
	Structural	375	0.13
	Resting fMRI	600	0.13

We note that we did not turn off the scanners cold-head. We found that this potential source of artefact in the icEEG data due to associated vibrations was not a strong enough effect to show a significant difference in the expected lower frequency range (e.g. delta–theta bands) but it may still contaminate the spectrum at specific frequencies and could explain the differences found at low gamma frequencies in one contact.

MRI data quality

MRI image quality was sufficient to allow us to detect highly significant task-related fMRI responses ($p<0.05$ FWE corrected) in close proximity (<2 mm) to some electrode contacts during a 5-minute block design motor task. GE-EPI signal reduction was confined to within 10 mm of the electrode contacts in all cases and on average >50% of signal intensity was available within 5 mm of the contact locations. Comparison of the GE-EPI images from the two subjects suggested dependence between the electrode-related GE-EPI signal degradation and electrode contact location and orientation. Comparison of the GE-EPI signal loss at 5 mm from the electrode contacts at various orientations relative to the main magnetic field demonstrated that GE-EPI signal reduction was related to the electrode contact angle; contacts with surface normal parallel to the B_0 field had a greater signal reduction. This suggests that the main contributor to GE-EPI signal loss was B_0 rather than radio frequency B_1 interactions which can also affect image quality (Mullinger et al., 2008). However, B_1 interactions remain an important potential source of image artefacts (Bennett et al., 1996; Mullinger et al., 2008) as are potential changes to the slice profile. Anatomically, this corresponded to electrode contacts closer to the midline and more posterior within the frontal grid in patient #1, and contacts that were going under the temporal pole in patient #2, suffering from greater GE-EPI signal degradation. The additional inter-electrode variability in GE-EPI signal loss in patient #2 is attributable to the brain surface topography at the temporal poles and basal-temporal areas where paths normal to the electrode contacts pass other contacts or have paths that are

not entirely within brain tissue. In this case the range is less informative but the mean GE-EPI signal reduction should be relatively unaffected by these few contacts.

fMRI protocol considerations for icEEG–fMRI

We used a standard GE-EPI sequence with minimum readout duration at 1.5 T, relatively thin slices (~2 mm effective slice thickness) and a relatively short echo time (TE = 40 ms). The latter was specified to provide close to optimal BOLD (blood oxygenation level dependent) sensitivity while reducing GE-EPI signal loss due to through-plane signal dephasing (Deichmann et al., 2002; Weiskopf et al., 2006) caused by electrode-related susceptibility gradients. We note that the reduced BOLD sensitivity due to shortened echo time (Deichmann et al., 2002) in GE-EPI will likely be attenuated when physiological noise is considered. Slice thickness was also chosen to reduce through-plane signal dephasing (Howseman et al., 1999; Weiskopf et al., 2006), while allowing for whole brain coverage and acceptable image signal-to-noise ratio (SNR). Further optimisation of these parameters may yield an incremental improvement in BOLD sensitivity in the presence of intracranial EEG electrodes.

Our choice of scanning at 1.5 T was motivated firstly by the reduced radio frequency power deposition (SAR) required (compared to an equivalent pulse sequence at 3 T) with a concomitant reduction in the risk of hazardous heating (Carmichael et al., 2008a, 2010). Secondly, at 1.5 T there is also reduced sensitivity to susceptibility related artefacts compared to 3 T for equivalent sequence parameters (Mullinger et al., 2008); these are suggested as being the predominant source of GE-EPI image degradation here.

Limitations of the current study

There is a limitation in the accuracy of the electrode localisation based on CT obtained 1–2 weeks earlier and the structural MRI image obtained in the same session, but suffering from some electrode-related artefacts albeit small in magnitude compared to those in the GE-EPI images. We estimate electrode contact localisation precision to be in the range 2–5 mm. The calculation of the average GE-EPI signal reduction should be relatively insensitive to these inaccuracies.

We have not attempted to separate the contributions of GE-EPI image distortion from signal loss. Distortion could be responsible at least partially for the variability seen in signal reductions with electrode location. To determine distortion requires the precise calculation of fast changing local magnetic fields around the electrodes and was beyond the scope of this study.

Eddy currents induced in the electrodes by either RF or gradient switching can potentially cause a spatial distribution of signal disturbance; quantitative field mapping and simulations would help to determine if these effects are a significant contributor to the EPI signal reduction described here.

Task-driven fMRI signal changes in GE-EPI images depend on a number of factors (Deichmann et al., 2002) which can be summarised via the BOLD sensitivity, a product of the local effective echo time and the local GE-EPI signal level. We have examined local GE-EPI signal level without quantifying the effective echo time and so only a qualitative estimate of the effect on measurable BOLD changes is possible. As mentioned above, we have chosen scan parameters based on our experience and data from previous studies on BOLD sensitivity and artefact minimisation. We observed task-driven fMRI signal changes under the electrode grid in case #1 suggesting that the image quality obtained was sufficient to enable BOLD changes to be measured both local to and distant from the sites of electrophysiological recordings in this case. We therefore anticipate that local BOLD changes to epileptic spikes can be detected using icEEG–fMRI given the data quality. However, the GE-EPI signal degradation seen in some locations may preclude recording fMRI signal changes reliably within close proximity to the electrodes. The volume of typical fMRI activations is also likely to be an important factor for detectability. We used standard spatial smoothing of 8 mm and the area of activation was large both in superficial and deeper brain structures where we measured robust fMRI signal changes. The fMRI data from parts of the brain distant from the electrode contacts can be seen as the most complimentary to icEEG in that the fMRI extends the brain volume covered compared to icEEG alone. Nevertheless co-localised icEEG and fMRI data (from around each electrode contact) are important for interpreting the local sensitivity of icEEG–fMRI and more generally for determining the local coupling between the two signals. It is likely that a combination of spin and gradient echoes or multiple gradient echoes with a z-shim will yield improved imaging performance local to the electrodes while providing acceptable BOLD sensitivity from the entire brain. Although careful sequence design will be needed to avoid substantially increasing SAR, and therefore reducing safety margins (Carmichael, 2010).

Conclusions

We have performed icEEG–fMRI using a 1.5 T MRI scanner with a head transmit–receive coil, low SAR sequences and electrode leads and wires external to the head with specific lengths and precisely positioned along the RF coil's central z-axis. In this configuration, heating in-vitro was limited to $\leq$0.1 °C, implying a safety factor of 10 in relation to the statutory temperature increase limits. In measurements in two patients icEEG quality during MRI was quantitatively comparable to recordings outside the MRI scanner with heart beat-related artefact typically 10–20 times smaller in magnitude relative to electrophysiological signals of interest. A GE-EPI image signal loss of less than 50% was found on average at 5 mm distance from electrode contacts, with signal loss confined within a 10 mm radius in GE-EPI images. The GE-EPI image signal loss appeared related to contact orientation relative to the main magnetic field (B_0); where contacts possessed a surface normal parallel to the B_0 field a greater signal reduction was measured. This information can be used to guide interpretation of results of icEEG–fMRI experiments proximal to the electrodes, and optimised strategies for image artefact reduction. Future studies are needed to maximise BOLD sensitivity both globally and locally to intracranial electrodes for the best MRI data quality and explore tailored pulse sequences.

Supplementary data to this article can be found online at http://dx.doi.org/10.1016/j.neuroimage.2012.05.056.

Acknowledgments

We are grateful to our colleagues in the Telemetry Unit and the Neuroradiology Department at the National Hospital for Neurology and Neurosurgery (UCLH), Queen Square, London UK for their help in data collection. DC, RR and LL acknowledge the financial support of the UK Medical Research Council (MRC grant G0301067). S. Vulliemoz was supported by a fellowship for advanced researcher and by the SNF grant 33CM30-124089 and 320030-141165 (SPUM Epilepsy) from the Swiss National Science Foundation. This work was undertaken at University College London Hospital/University College London (UCLH/UCL) who received a proportion of funding from the Department of Health's NIHR Biomedical Research Centres funding scheme. The support of Action Medical Research and The James Tudor Trust is also acknowledged.

References

Allen, P.J., Polizzi, G., Krakow, K., Fish, D.R., Lemieux, L., 1998. Identification of EEG events in the MR scanner: the problem of pulse artifact and a method for its subtraction. Neuroimage 8, 229–239.

Allen, P.J., Josephs, O., Turner, R., 2000. A method for removing imaging artifact from continuous EEG recorded during functional MRI. Neuroimage 12, 230–239.

Bennett, L.H., Wang, P.S., Donahue, M.J., 1996. Artifacts in magnetic resonance imaging from metals. J. Appl. Phys. 79, 4712–4714.Carmichael, D.W., Pinto, S., Limousin-Dowsey, P., Thobois, S., Allen, P.J., Lemieux, L., Yousry, T., Thornton, J.S., 2007. Functional MRI with active, fully implanted, deep brain stimulation systems: safety and experimental confounds. Neuroimage 37, 508–517.

Carmichael, D.W., 2010. Image quality issues. In: Mulert, C., Lemieux, L. (Eds.), EEG-fMRI: Physiological Basis, Technique, and Applications. Springer, Heidelberg, pp. 173–194.

Carmichael, D.W., Pinto, S., Limousin-Dowsey, P., Thobois, S., Allen, P.J., Lemieux, L., Yousry, T., Thornton, J.S., 2007. Functional MRI with active, fully implanted, deep brain stimulation systems: safety and experimental confounds. Neuroimage 37 (2) Aug 15, 508–517.

Carmichael, D.W., Thornton, J.S., Rodionov, R., Thornton, R., McEvoy, A., Allen, P.J., Lemieux, L., 2008a. Safety of localizing epilepsy monitoring intracranial electroencephalograph electrodes using MRI: radiofrequency-induced heating. J. Magn. Reson. Imaging 28, 1233–1244.

Carmichael, D.W., Hand, J., Li, Y., McEvoy, A., Lemieux, L., 2008b. Estimating specific absorption rate (SAR) during MRI in the human brain with intracranial EEG electrodes used for epilepsy monitoring: a preliminary study using finite integral technique (FIT) modelling. Proc. International Meeting of the ISMRM (Toronto), p. 1061.

Carmichael, D.W., Thornton, J.S., Rodionov, R., Thornton, R., McEvoy, A.W., Ordidge, R.J., Allen, P.J., Lemieux, L., 2010. Feasibility of simultaneous intracranial EEG-fMRI in humans: a safety study. Neuroimage 49, 379–390.

Deichmann, R., Josephs, O., Hutton, C., Corfield, D.R., Turner, R., 2002. Compensation of susceptibility-induced BOLD sensitivity losses in echo-planar fMRI imaging. Neuroimage 15, 120–135.

Dewhirst, M.W., Viglianti, B.L., Lora-Michiels, M., Hanson, M., Hoopes, P.J., 2003. Basic principles of thermal dosimetry and thermal thresholds for tissue damage from hyperthermia. Int. J. Hyperthermia 19, 267–294.

Howseman, A.M., Grootoonk, S., Porter, D.A., Ramdeen, J., Holmes, A.P., Turner, R., 1999. The effect of slice order and thickness on fMRI activation data using multislice echo-planar imaging. Neuroimage 9, 363–376.

International Electrotechnical Commission (IEC), 2002. Medical electrical equipment — particular requirements for the safety of magnetic resonance equipment for medical diagnosis. IEC 60601-2-33.

Mattei, E., Triventi, M., Calcagnini, G., Censi, F., Kainz, W., Bassen, H.I., Bartolini, P., 2007. Temperature and SAR measurement errors in the evaluation of metallic linear structures heating during MRI using fluoroptic probes. Phys. Med. Biol. 52 (6), 1633–1646 (Mar 21).

Mullinger, K., Debener, S., Coxon, R., Bowtell, R., 2008. Effects of simultaneous EEG recording on MRI data quality at 1.5, 3 and 7 Tesla. Int. J. Psychophysiol. 67 (3), 178–188.

Tao, J.X., Ray, A., Hawes-Ebersole, S., Ebersole, J.S., 2005. Intracranial EEG substrates of scalp EEG interictal spikes. Epilepsia 46, 669–676.

Vulliemoz, S., Carmichael, D.W., Rosenkranz, K., Diehl, B., Rodionov, R., Walker, M.C., McEvoy, A.W., Lemieux, L., 2011. Simultaneous intracranial EEG and fMRI of interictal epileptic discharges in humans. Neuroimage 54, 182–190.

Weiskopf, N., Hutton, C., Josephs, O., Deichmann, R., 2006. Optimal EPI parameters for reduction of susceptibility-induced BOLD sensitivity losses: a whole-brain analysis at 3 T and 1.5 T. Neuroimage 33, 493–504.